# Transparent, Broadband, Flexible, and Bifacial-Operable Photodetectors Containing a Large-Area Graphene–Gold Oxide Heterojunction

Yu-Lun Liu,[†] Chen-Chieh Yu,[†] Keng-Te Lin,[†] Tai-Chi Yang,[†] En-Yun Wang,[†] Hsuen-Li Chen,[*,†] Li-Chyong Chen,[‡] and Kuei-Hsien Chen[‡,§]

[†]Department of Materials Science and Engineering, National Taiwan University, Taipei, 10617 Taiwan, R.O.C., [‡]Center for Condensed Matter Sciences, National Taiwan University, Taipei, 10617 Taiwan, R.O.C., and [§]Institute of Atomic and Molecular Sciences, Academia Sinica, No. 1, Sec. 4, Roosevelt Road, Taipei, 10617 Taiwan, R.O.C.

**ABSTRACT** In this study, we combine graphene with gold oxide ($AuO_x$), a transparent and high-work-function electrode material, to achieve a high-efficient, low-bias, large-area, flexible, transparent, broadband, and bifacial-operable photodetector. The photodetector operates through hot electrons being generated in the graphene and charge separation occurring at the $AuO_x$–graphene heterojunction. The large-area graphene covering the $AuO_x$ electrode efficiently prevented reduction of its surface; it also acted as a square-centimeter-scale active area for light harvesting and photodetection. Our graphene/$AuO_x$ photodetector displays high responsivity under low-intensity light illumination, demonstrating picowatt sensitivity in the ultraviolet regime and nanowatt sensitivity in the infrared regime for optical telecommunication. In addition, this photodetector not only exhibited broadband (from UV to IR) high responsivity—3300 A $W^{-1}$ at 310 nm (UV), 58 A $W^{-1}$ at 500 nm (visible), and 9 A $W^{-1}$ at 1550 nm (IR)—but also required only a low applied bias (0.1 V). The hot-carrier-assisted photoresponse was excellent, especially in the short-wavelength regime. In addition, the graphene/$AuO_x$ photodetector exhibited great flexibility and stability. Moreover, such vertical heterojunction-based graphene/$AuO_x$ photodetectors should be compatible with other transparent optoelectronic devices, suggesting applications in flexible and wearable optoelectronic technologies.

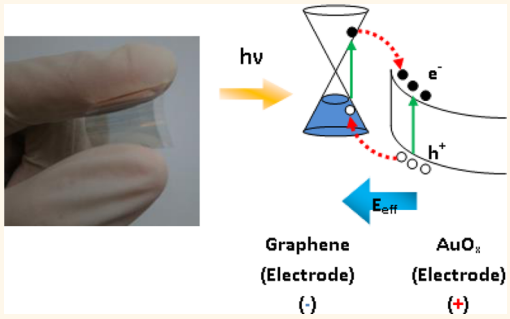


**KEYWORDS:** gold oxide ($AuO_x$) · graphene · transparent · photodetector · heterojunction · flexible device · bifacial operation

Large-area, highly efficient, flexible, transparent, and broadband-operable photodetectors are of interest for the development of novel optoelectronic systems. Photodetectors are key components in optoelectronic systems; although several based on conventional semiconductor materials (*e.g.*, silicon) have demonstrated high efficiency,[1,2] there remain some issues that should be overcome. First, the responsivity of those photodetectors has been extremely low when working below the band gap of the semiconductor, generally limiting their efficiency in the long-wavelength regime because of band-gap restriction. Second, broadband-responsive photodetectors that can be operated at room temperature from the ultraviolet to the infrared regime are rare. Third, most semiconductors are opaque and incompatible with flexible substrates, thereby restricting their applications in wearable devices. Accordingly, the development of broadband-operable, transparent, highly efficient, and flexible photodetection devices remains a great challenge for the development of future optoelectronic systems.

Graphene has attracted much attention because of its zero-gap, linear band structure and unique photonic properties, allowing rapid operation and broadband absorption of light.[3] In addition to having electron mobility superior to that of conventional semiconductor materials, the flexibility of graphene makes it a promising candidate material for use in flexible electronics.[4] On the basis of excitation of electron/hole pairs from its single-atom-thick carbon layer, the broadband photoresponses of graphene-based photodetectors

* Address correspondence to hsuenlichen@ntu.edu.tw.

Received for review January 12, 2015 and accepted April 23, 2015.

**Published online April 30, 2015**
10.1021/acsnano.5b00212

are superior to those of other semiconductor materials.[3]

Although graphene has great potential for application in photodetection, most such studies have involved complicated device structures and small detection areas, seriously restricting practical applications. The literature describes various photodetection architectures, including phototransistor-type, junction-type, and photoconductor-type systems.[5−9] Traditionally, gated graphene photodetectors featuring three terminals have been prepared using complicated processes, and it has been difficult to achieve large-area, transparent devices. Moreover, the need to apply an electric field generated from the gate voltage restricts the use of some insulating substrates. The simplest configuration reported previously is based on a metal−graphene−metal (MGM) configuration, consisting of only two conducting electrodes.[10,11] These kinds of devices are easy to fabricate and also suitable for the fabrication of large-area photosensors.[12] The current performance of graphene-based devices is, however, relatively poor because of the intrinsic limitations arising from its inherently low absorption (*ca.* 2.3%). Graphene samples integrated with optical antennas and plasmonic structures have been used in a variety of fields, including subwavelength optics, surface-enhanced spectroscopy, and sensing; the optical antennas and plasmonic structures help the graphene to harvest visible and near-IR light with higher efficiency.[13−15] Moreover, such enhancements in light harvesting ability can be achieved only under the designed resonant frequency, restricting broadband applications. Accordingly, the challenge remains to develop graphene-based, broadband- and room-temperature-operable photodetectors through simple fabrication processes.[16]

In addition to improving absorption, exploiting interfacial interactions is an alternative means of enhancing the photogain of graphene-based devices. For example, a built-in electric field can accelerate the photocurrent generated at graphene−metal contacts.[17] Recently, various methods have been reported to construct graphene-based hybrids for photodetection. Zhang *et al.* prepared photodetectors based on the $MoS_2$/graphene system, observing charge movement in the built-in electric field within the two-dimensional heterostructures.[18] Such vertical heterostructures can significantly increase the responsivity of devices. Yu *et al.* found that vertical heterostructures of graphene−$MoS_2$−graphene stacks could create high photocurrents through a dual-gated structure.[19] The influence of the carrier doping effect provides a high photogain, due to charge transfer at the junction surface, enabling highly efficient separation of electron/hole pairs because of the built-in electric field provided by the graphene/metal contacts.

In previous studies, metal electrodes have been used to induce charge separation between the graphene and the electrodes; a challenge is, therefore, selecting the best electrodes.[20] The difference in work function between the graphene and the electrode will greatly influence the charge-transfer properties in graphene-based devices and will induce charge-transfer doping beneath the contact metals and adjacent regions in the graphene channel. Therefore, the selection of a suitable metal electrode is a key factor affecting improvements in device performance. The highest photoresponsivity of a graphene-based device (*ca.* 6.1 mA $W^{-1}$) was that reported by Xia and Mueller *et al.*, who employed an asymmetric metallization scheme.[10] In recent years, the design of graphene-based photodetectors has usually been based on lateral MGM junctions having a small, inhomogeneous active area, which cannot perform effective light harvesting.[11] The small active area limits the responsivity of lateral MGM photodetectors; in addition, high bias must be applied to these devices. Recently, a transparent graphene-based device was demonstrated for IR photodetection.[21] Liu *et al.* proposed a method for making a large-area photodetector based on the controllable fabrication of lateral P−N junctions on graphene.[21] The processes for fabricating this type of graphene-based device are, however, complicated and time-consuming. When preparing their device, Liu *et al.* subjected the layer of graphene to multiple photolithography processes, with accurate alignment required to define the distance to the electrode and the area of the P/N-type graphene. Furthermore, the photoelectric performance of P−N junction-based graphene devices would be affected significantly by the distance to the electrode, due to the limited depletion length of a P−N junction. Moreover, the generated photocurrent-to-dark current ratio of that graphene-based device was only 5%, even when applying a large bias voltage of 5 V. Therefore, we suspect that the stacking of layered graphene on metal electrodes (vertical heterojunctions) will enable the formation of large active areas, while enhancing the light−graphene interaction and improving the responsivity of devices.

Bifacial photodetectors can be prepared at low cost with the capability of detecting illuminating signals on both sides. Moreover, the transparency of bifacial photodetectors renders them highly promising devices for building integrated dual-side working systems. Recently, a graphene-based bifacial solar cell was demonstrated.[22] Nevertheless, bifacial photodetectors on flexible substrates have not been demonstrated previously. In this study, we combined graphene with a high-work-function electrode, gold oxide ($AuO_x$), for use as a vertical heterojunction to achieve a large-area, bifacial-operable, highly efficient graphene-based photodetector.

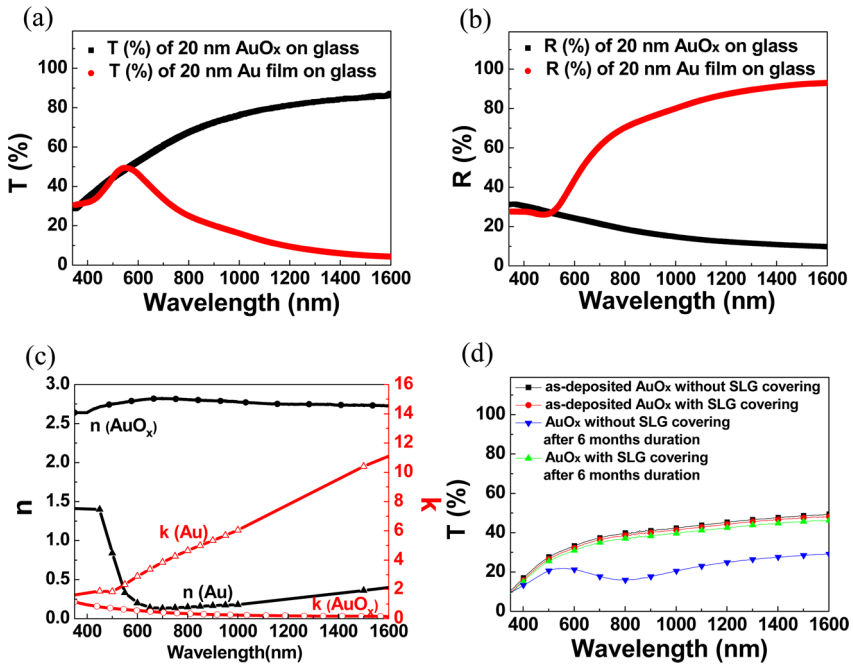


**Figure 1. (a) Transmittance and (b) reflectance spectra of as-deposited 20 nm thick $AuO_x$ and pure Au films on glass substrates. (c) Optical constants of $AuO_x$ and pure Au films. (d) Transmittance of $AuO_x$ films, with and without the covering of graphene, after six-month exposure to ambient conditions.**

Because $AuO_x$ possesses a high work function (*ca.* 5.5 eV) and low surface reflectance, it is a promising candidate material for use as electrodes.[23] The transparency and efficiency can both be preserved when incorporating $AuO_x$ in transparent devices. Recent studies have revealed that $AuO_x$ electrodes also possess high work functions and high flexibility and are compatible with optoelectronic devices for use as hole-injection layers in organic light-emitting diodes (OLEDs).[24] $AuO_x$ can be applied as an electrode for hole injection because it is commonly believed that a high-work-function electrode leads to low hole injection barriers.[23,24] In a previous study, we investigated the optical properties of $AuO_x$.[25] In addition, we found we could deposit large-area $AuO_x$ films, with reduction from $AuO_x$ to Au films arising due to the desorption of molecular oxygen, a process that could be monitored using conventional transmission and reflection spectra.[25] Therefore, preventing the desorption of oxygen requires a strong protective layer impermeable to $O_2$ gas. Because graphene is impermeable to gases such as helium,[26] we suspected that a covering of graphene on the $AuO_x$ surface would prevent the reduction of $AuO_x$ and, thereby, extend the functionality of the $AuO_x$ electrode under general ambient conditions. We are unaware of any previous investigations into the stability of $AuO_x$ in the presence of graphene or of any combining graphene with $AuO_x$ in a single device for applications in light detection. Relative to previously reported graphene-based devices, we suspected that graphene/$AuO_x$ devices featuring two-dimensional junctions with high intrinsic carrier mobility would have greater probability of receiving photons and, thereby, would provide larger photoinduced electric currents, potentially leading to practical transparent, broadband-operable photodetectors having large detection areas.

In this paper, we demonstrate a large-area, flexible, transparent, broadband- and bifacial-operable graphene/$AuO_x$ photodetector on a polyethylene terephthalate (PET) substrate. When applying a low bias voltage (0.1 V), the high work function and transparency of the $AuO_x$ electrode allowed effective charge separation. We demonstrate the high responsivity of this graphene/$AuO_x$ photodetector from the UV to the IR regime used for optical telecommunication. We also found that the internal quantum efficiency (IQE), related to the contribution of hot carriers in the graphene, was strongly dependent on the excitation wavelength. Moreover, the device exhibited high stability during a bending test. In this simple vertical-heterojunction structure, the graphene functioned as an active layer, providing flexibility and broadband-operable photodetection. This transparent, flexible, highly efficient, bifacial, broadband-operable graphene/$AuO_x$ photodetector appeared to have great potential for future use in smart devices.

## RESULTS AND DISCUSSION

To characterize the optical properties of various electrodes, we first deposited Au and $AuO_x$ films of the same thickness onto glass substrates for optical measurements. Figure 1a and b display the UV–vis–IR transmittance and reflectance spectra of 20 nm thick

Au and $AuO_x$ films, respectively. The high transmittance of the $AuO_x$ film relative to that of the Au film confirmed the potential of the former for use as a transparent electrode in optoelectronic devices. Moreover, we used the optical thin film model to fit the measured spectroscopic ellipsometry data, thereby obtaining detailed optical constants [refractive index (*n*), extinction coefficient (*k*)]. The optical constants of the Au and $AuO_x$ films (Figure 1c) were quite distinct. For example, the $AuO_x$ film exhibited a much smaller extinction coefficient and a larger refractive index than those of the Au film in the visible-to-IR regime. $AuO_x$ films possessing high work functions have been used previously as hole-transporting layers in OLEDs.[24] The flexibility of $AuO_x$ compounds arises from the weak interactions between O and Au atoms. Nevertheless, as indicated in previous studies, $AuO_x$ films are not as stable as pure Au films, and oxygen desorption can induce the reduction of $AuO_x$ to generate Au nanoparticles (NPs) on the $AuO_x$ surface.[25] To overcome these drawbacks, we placed a covering of gas- and water-impermeable graphene onto the $AuO_x$ surface and tested the stability of the as-covered $AuO_x$ film. First, we deposited a $AuO_x$ film (40 nm) onto a glass substrate and then transferred CVD-prepared single-layer graphene (SLG) onto the $AuO_x$ surface. To investigate the stabilities of the $AuO_x$ films, we measured the transmittances and reflectance of the $AuO_x$ films with and without the covering of graphene, before and after exposure to the ambient environment for six months.

Figure 1d displays the transmittance spectra of $AuO_x$ films with and without the covering of SLG. A slight decrease in the transmittance (*ca.* 3%) occurred when the as-deposited $AuO_x$ film was covered with the SLG, due to the absorption of the latter. After six months of exposure to the atmosphere, the transmittance spectrum of the $AuO_x$ film without the covering of graphene revealed an obvious transmission dip at a wavelength of approximately 790 nm, originating from localized surface plasmon resonance of Au NPs obtained through reduction of the $AuO_x$.[25] In contrast, the transmittance of the $AuO_x$ film covered with graphene remained almost unchanged after six months of exposure to air, suggesting that the top-layer graphene suppressed reduction of the $AuO_x$ film, thereby potentially extending the practical applications of $AuO_x$ materials. In addition, such transmittance measurements allowed the ready real-time characterization of the reduction of $AuO_x$ films in a nondestructive manner.

To further analyze the ability of using this system for photodetection, we fabricated a vertical heterojunction-based photodetector comprising the SLG and transparent $AuO_x$ electrode on a flexible PET substrate. Figure 2a displays a schematic representation of the fabrication process. First, we sputtered a 20 nm thick $AuO_x$ film onto a 100 $\mu$m thick PET substrate. Subsequently, CVD-grown SLG was transferred onto the $AuO_x$ film using the conventional PMMA-mediated process. The PMMA layer was then dissolved in acetone and removed. To demonstrate large-area detection, here we transferred large-area graphene having an area of *ca.* $20 \times 10$ mm$^2$ onto the $AuO_x$ film. Finally, we deposited an individual 50 nm thick Ag contact on the edge of the graphene surface to ensure stable electrical measurements. Figure 2b displays a photographic image of the graphene/$AuO_x$ photodetector; each part of the device is outlined by dashed lines. Moreover, this graphene/$AuO_x$ photodetector exhibited high flexibility and transparency (Figure 2c). The underlying $AuO_x$ film and Ag contacts acted as the top and bottom electrodes, respectively. Figure 2d presents the transmittance and reflectance spectra of the SLG/$AuO_x$ system. Because of the low absorption of SLG, the transmittance and reflectance spectra of the graphene/20 nm thick $AuO_x$ photodetector are very similar to that of the 20 nm thick $AuO_x$ film itself (Figure 1a and b). For comparison, we also prepared a graphene/10 nm thick $AuO_x$ photodetector. The transmittance spectra revealed broadband transparency of the photodetector in the visible-to-IR regime, with the transmittance of 10 and 20 nm thick $AuO_x$/graphene-based photodetectors in the visible regime (400−750 nm) being approximately 64% and 49%, respectively. Moreover, the reflectance of each photodetector in the IR regime was lower than that in the visible regime, due to the lower extinction coefficients (*ca.* 0.15) of $AuO_x$ films in the IR regime. In addition, the absorbances of the 20 nm thick $AuO_x$/graphene photodetector in the UV and IR regimes were approximately 45.1% and 6.7%, respectively. Although the transmittance of the 10 nm thick $AuO_x$/graphene photodetector was higher than that of the 20 nm thick one, we consider the performance of only the 20 nm thick $AuO_x$/graphene photodetector in the following discussion because of its larger absorption and greater electrical performance.

To obtain insight into the material properties, as displayed in Figure 3, we used Raman spectroscopy to analyze the interactions of graphene with the $AuO_x$ film and other substrates. Recently, Entani *et al.* reported that the Raman shift of SLG is strongly dependent on the underlying substrate.[29] For comparison, we also fabricated suspended graphene (no substrate), without any doping interactions with the substrate. Typically, the Raman spectrum of graphene features two prominent bands: the G band (1580 cm$^{-1}$) and the 2D (2640 cm$^{-1}$) band (inset to Figure 3a). In this spectrum, the ratio of the intensity of the 2D and G bands is greater than 2, typical of an SLG. Figure 3a displays the G bands in the Raman spectra of SLGs on various substrates (air, $SiO_2$/Si, pure Au, $AuO_x$). Previous reports have suggested that shifts in the G band of the Raman peak can be attributed to doping effects from

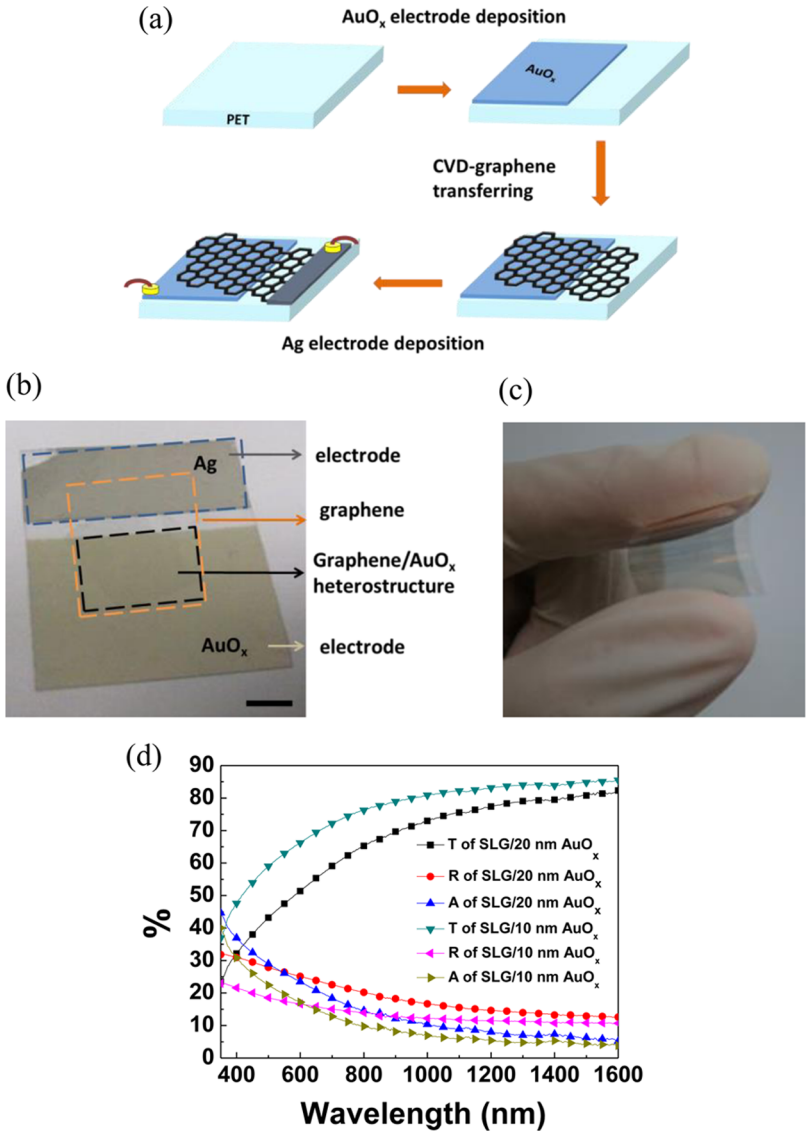


**Figure 2. (a) Schematic representation of the fabrication of a graphene/$AuO_x$ vertical heterostructure on a PET substrate. (b) Photograph of the graphene/$AuO_x$ photodetector; scale bar: 10 mm. (c) Photograph revealing the flexibility and transparency of the graphene/$AuO_x$ photodetector. (d) Transmittance, reflectance, and absorbance spectra of graphene/$AuO_x$ systems having various thicknesses of the $AuO_x$ layer on PET substrates.**

the underlying substrates.[29,30] A shift of the peak to larger wavenumber indicates an increase in the concentration of holes. As displayed in Figure 3a, the PMMA-transferred graphene was intrinsically p-type, with the peak shifting to larger wavenumbers on the different substrates, an obvious substrate-doping effect that would lead to shifting of the Fermi level. We found that the peak shift was most significant when we transferred the graphene onto the $AuO_x$ film, relative to those on the $SiO_2$/Si and pure Au substrates. The difference in work functions between the graphene and the substrate will greatly influence the surface-doping of the graphene, with a high-work-function substrate inducing large shifts of the G band and the Fermi level.[17] The G band of the graphene on the $AuO_x$ film appeared at a larger wavenumber than that of the graphene on the Au film, suggesting that the work function of the $AuO_x$ film was higher than that of the Au film. These results also implied that the hole-doping effect on the graphene surface was much more pronounced after transferring the graphene onto the $AuO_x$ film, thereby providing a better atomic junction between them. Figure S1 in the Supporting Information demonstrates the Hall measurement results of graphene doped by $AuO_x$. Figure 3b provides a schematic representation of heterojunction-assisted photodetection.[35] When the light is incident into the device, both graphene and $AuO_x$ could absorb the incident light and generate electron−hole pairs (e−h pairs). In addition, the $AuO_x$, which possesses larger absorbance, would generate more e−h pairs. The direction of the effective electric field is from $AuO_x$ to graphene (combined with built-in electric field and applied bias voltage), which makes the generated

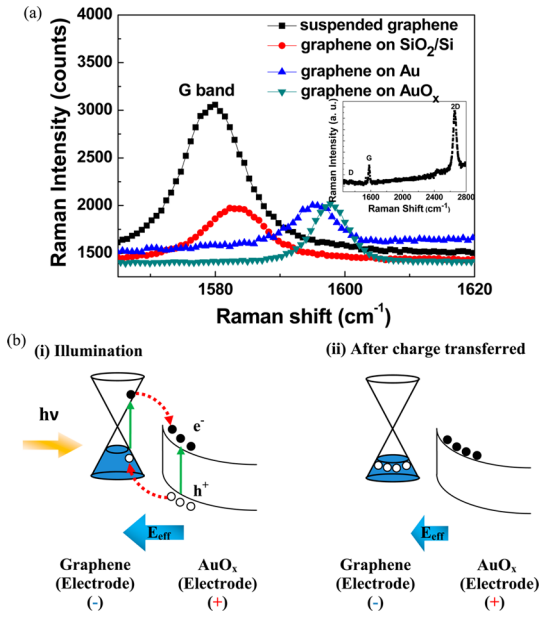


**Figure 3. (a) Raman spectra (G band region) of SLGs on various substrates. Inset: Raman spectrum of suspended graphene with significant G and 2D bands. (b) (i) Schematic band diagram of the graphene−$AuO_x$ heterojunction; the effective electric field ($E_{eff}$) assists in separating the electron/hole pairs under illumination with light. (ii) After graphene obtains holes, an electric field of the opposite direction is produced to cancel out the original electric field so that the photocurrent gradually reaches saturation.**

holes in $AuO_x$ transfer into graphene so that the photocurrent increases. The influence of such a carrier doping effect would provide a high photogain.[16,18,36] After graphene obtains holes, an electric field of the opposite direction is produced to cancel out the original electric field so that the photocurrent gradually reaches saturation.

To further investigate the photoresponse of our graphene/$AuO_x$ photodetector, we measured the current−voltage ($I$−$V$) characteristics at room temperature while illuminating with light ($\lambda$ = 500 nm, red curve) and without illumination (black curve) (Figure 4a). We attribute the enhanced current (excess current) under illumination to the generation of photoexcited charge carriers and charge transferring between graphene and $AuO_x$ (Figure 4a), confirming that an atomic junction had formed at the graphene−$AuO_x$ interface. The resulting effective electric field could help facilitate the separation of the photogenerated electron/hole pairs. Thus, the graphene/$AuO_x$ photodetector could readily achieve high photoresponsivity without applying a high external bias voltage.

The graphene/$AuO_x$ photodetector displayed a broadband photoresponse. Figure 4b presents the bias-dependent responsivity of the graphene/$AuO_x$ photodetector under illumination with light at wavelengths of 310 nm (UV), 500 nm (visible), 850 nm (near IR), and 1550 nm (IR). The incident light power was fixed at 1 $\mu$W for each of the different wavelengths of incident light. The graphene/$AuO_x$ system exhibited photoresponses from the UV to the IR regime, associated with the broadband absorption properties of graphene and $AuO_x$ (Figure 2d). As we increased the bias from −0.1 to +0.1 V, the responsivity rose accordingly and linearly. Compared with other three-terminal gated devices, our graphene/$AuO_x$ photodetector achieved high responsivity without the need for gate-voltage doping; therefore, it appears much more suitable for use in transparent devices. For comparison, we also fabricated a graphene/pure Au photodetector of the same thickness. Because of more charge transferring at the graphene−$AuO_x$ interface, as displayed in Figure 4b, the responsivity of the graphene/$AuO_x$ photodetector was always higher than that of the graphene/Au photodetector at a fixed bias. Notably, the responsivity of the graphene/$AuO_x$ photodetector was higher under UV irradiation than under visible or IR irradiation at the same bias, consistent with the absorbance behavior displayed in Figure 2d. Figure 4c summarizes the wavelength-dependent responsivities of the graphene/$AuO_x$ heterostructure, the graphene/Au heterostructure, and the $AuO_x$ film at a fixed bias of 0.1 V under an incident power of 1 $\mu$W. Among our tested structures, the graphene/$AuO_x$ heterostructure exhibited the broadest and highest responsivities from the UV to the IR regimes; indeed, its performance was much superior to those of the other two structures. In addition, the graphene/$AuO_x$ photodetector demonstrated an enhancement in responsivity of approximately 10-fold relative to that of the graphene/Au photodetector in the broadband spectral regime. Notably, the $AuO_x$ film alone exhibited no photoresponse under a bias of 0.1 V (Figure 4c). Therefore, the high excess current of the graphene/$AuO_x$ device must have arisen from the presence of graphene and the graphene−$AuO_x$ junction.

Figure 4d presents the responsivity of the graphene/$AuO_x$ photodetector illuminated from different sides of the device at a fixed incident power of 1 $\mu$W. Both front- and rear-side illumination induced apparent photoresponsivity, revealing the bifacial working capability of this graphene/$AuO_x$ photodetector. Relative to the responsivity during front-side illumination, the responsivity during rear-side illumination was relatively low, due to the absorption of the $AuO_x$ electrode partially blocking the light. Moreover, the difference in responsivity between front- and rear-side illuminations was relatively large at wavelengths of 500 and 1550 nm, due to the high transparency of the $AuO_x$ electrode in the visible and IR regimes. Nonetheless, the graphene/$AuO_x$ photodetector did display apparent dual-side responsivities in both the visible and IR regimes. Such bifacial operability would substantially decrease the cost of using the photodetector on different sides and would broaden the applications of such flexible and transparent photodetectors.

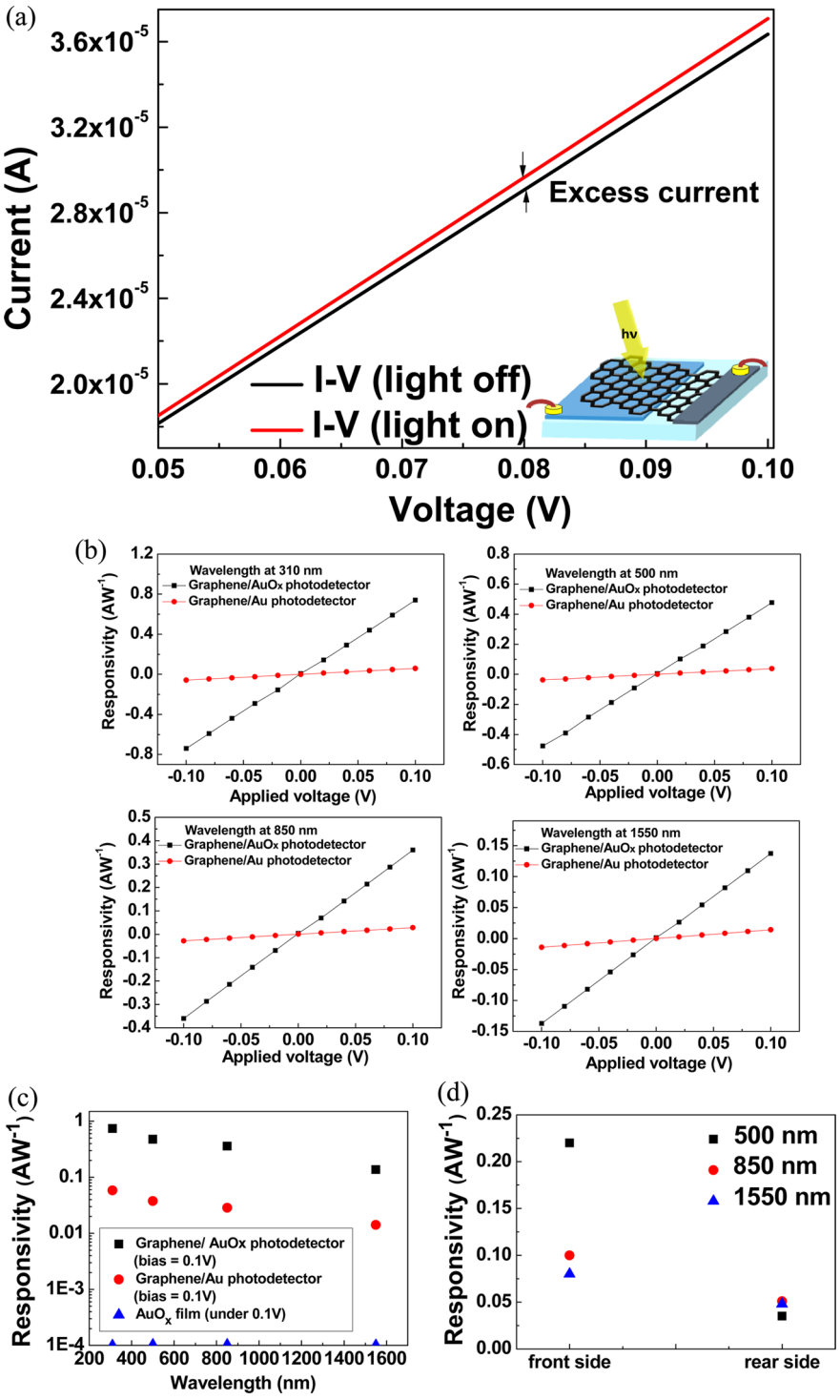


**Figure 4. (a) Current−voltage characteristics of the graphene/$AuO_x$ photodetector in the presence and absence of light ($\lambda$ = 500 nm; power = 1 $\mu$W). (b) Responsivities of graphene/$AuO_x$ and graphene/Au photodetectors, plotted with respect to the bias, under incident light of various wavelengths, at a fixed incident power of 1 $\mu$W. (c) Wavelength-dependent responsivities of graphene/$AuO_x$ and graphene/Au photodetectors and a $AuO_x$ film, at a fixed incident power of 1 $\mu$W. (d) Responsivities of the graphene/$AuO_x$ photodetector measured during front- and rear-side illumination.**

Figure 5 displays plots of the incident power-dependent excess current and responsivity for the graphene/$AuO_x$ photodetector under light at wavelengths of 310, 500, and 1550 nm. In the UV regime (310 nm), the excess current responded linearly when the incident power was in the range of several hundred picowatts (Figure 5a). Remarkably, the photodetector exhibited a wide range of photoresponses even when the incident power was as low as the picowatt level. In addition, when the incident power was high, the excess current saturated at approximately 1 $\mu$A. This phenomenon of excess current saturation has been

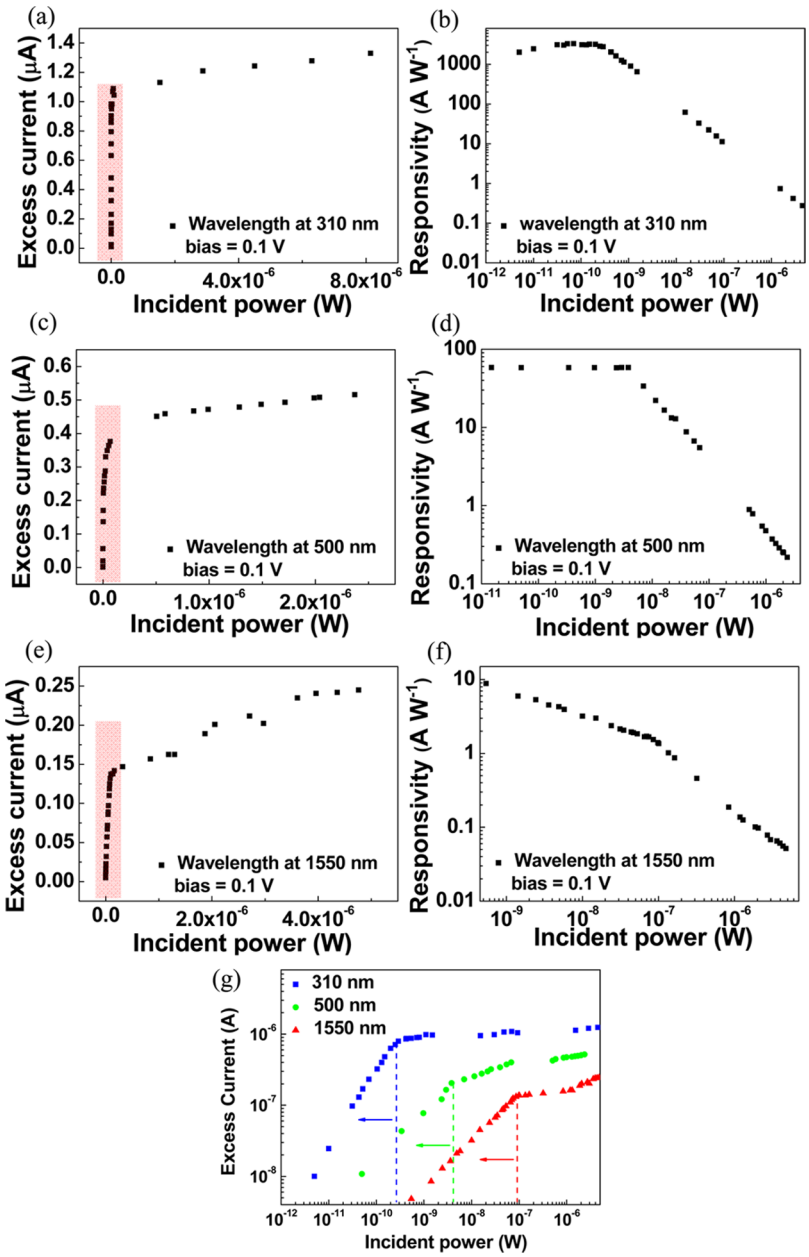


**Figure 5. (a–f) Plots of (a, c, e) excess current and (b, d, f) responsivity with respect to the incident power, under incident light having wavelengths of (a, b) 310, (c, d) 500, and (e, f) 1550 nm, at a fixed bias of 0.1 V; red-shaded rectangular regimes in (a, c, e) highlight the regions of linear response. (g) Logarithmic-scale comparison of the incident power-dependent excess current under light of various wavelengths.**

observed for other graphene-based photodetectors; it is due to a screening effect, similar to that found in conventional photodiodes.[10,19,31] The presence of trap states in graphene, or at the graphene–$AuO_x$ electrode interface, may have been responsible for this current saturation. In addition, the charge transferring between graphene and $AuO_x$ makes the effective electric field decrease, so the photocurrent will saturate in the end. The power-dependent excess currents under visible ($\lambda$ = 500 nm; Figure 5c) and IR ($\lambda$ = 1550 nm; Figure 5e) light displayed similar phenomena to that in the UV regime, with the excess current becoming saturated under light of high incident power; the saturation currents under light at 500 and 1550 nm were approximately $2 \times 10^{-7}$ and $1 \times 10^{-7}$ A, respectively. Figure 5g summarizes the incident power-dependent excess currents on a logarithmic scale. For incident light at wavelengths of 310, 500, and 1550 nm, the thresholds of detectable power were approximately $2 \times 10^{-10}$, $3 \times 10^{-9}$, and $1 \times 10^{-7}$ W, respectively. In addition, the saturation excess current in the UV regime (1 $\mu$A) was higher than those obtained in the visible (0.2 $\mu$A) and IR (0.1 $\mu$A) regimes. This unique phenomenon may be due to efficient hot-carrier collisions in the UV regime.[32,33] Moreover, the threshold of detectable

power in the UV regime was lower than those in the visible and IR regimes, suggesting higher efficiency for carrier multiplication when irradiating with UV light.

Moreover, the graphene/$AuO_x$ photodetector exhibited remarkable responsivity of approximately 3300 A $W^{-1}$ (Figure 5b) at low incident power (a few tens of picowatts) in the UV regime. This value is several orders of magnitude higher than those of previously reported graphene/metal-based photodetectors.[10,11] Accordingly, this graphene/$AuO_x$ system having a vertical heterostructure could more efficiently convert photon energy into electrical signals. Under an incident power of *ca.* $10^{-10}$ W, the visible and IR responsivities of the photodetector were 58 A $W^{-1}$ (Figure 5d) and 9 A $W^{-1}$ (Figure 5f), respectively. Therefore, this detector exhibited both ultrahigh responsivity in the UV regime and superior performance in both the visible and IR regimes, relative to those of previously reported systems. The techniques used previously to enhance the photoresponses in the visible and IR regimes have focused mainly on complicated plasmonic and waveguide structures, which are not practical for preparing large-area photosensors.[13−15] On the basis of the absorbance spectra in Figure 2d, the absorbance in the UV regime (45.1%) was only 1.5 and 6.7 times those in the visible (29.3%) and IR (6.7%) regimes. Therefore, the ultrahigh responsivity in the UV regime may have been due to the high photon energy of UV light, which would contribute to more hot carriers being generated in the graphene. Nonetheless, under a low bias of 0.1 V, the graphene/$AuO_x$ photodetector exhibited responsivities of 58 and 9 A $W^{-1}$ at wavelengths of 500 and 1550 nm, respectively, sufficiently high for a high-performance, inexpensive, room-temperature-operable photodetector in the visible and optical telecom regimes.

Next, we investigated the IQEs of the vertical-heterojunction graphene/$AuO_x$ photodetector (Figure 6a), measured at a fixed bias of 0.1 V under incident light of various wavelengths and photon intensities. We found that the IQE of the device was highly dependent on the photon density. The IQE describes the efficiency of hot-carrier generation in the photodetector under various absorbed photon densities. We found that the IQE decreased upon increasing the absorbed photon density, consistent with the trend in the responsivity of the device. IQEs exceeding 100% indicated that additional electron−hole pairs were generated during the carrier−carrier scattering process, which resulted in the creation of secondary hot carriers. We also compared the IQEs under incident light of various wavelengths. At the same absorbed photon density, the IQE under UV light was much higher than those under visible and IR light. Because of the higher photon energy, hot-carrier generation was more efficient in the UV regime.[34] In addition, remarkably high IQEs (from *ca.* $10^4$ to $10^6$%) in the UV regime suggest that

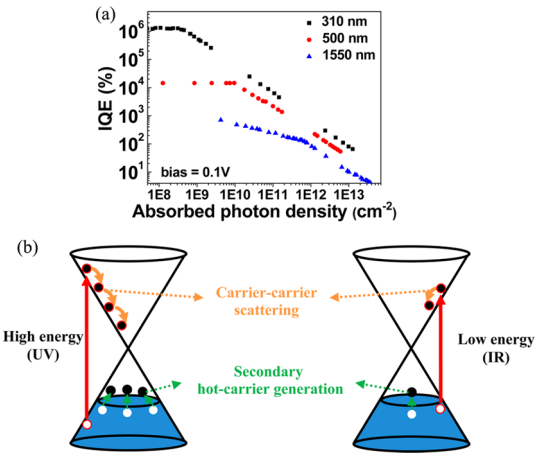


**Figure 6. (a) IQEs of the graphene/$AuO_x$ photodetector plotted with respect to the absorbed photon density, under light of various wavelengths, at a fixed bias of 0.1 V. (b) Schematic representation of additional electron/hole pairs generated during carrier−carrier scattering processes, where the energy was transferred to multiple secondary hot carriers.**

the graphene/$AuO_x$ photodetector has great potential for applications requiring detection of ultra-low-intensity light in the UV regime. Moreover, the IQEs of the graphene/$AuO_x$ heterostructure are much higher than those observed previously for lateral MGM-based photodetectors.[10] The ultrahigh IQEs arose not only from very efficient photon absorption within the large area of the vertical heterojunction but also from highly efficient charge separation and the hot-carrier-assisted mechanism, as illustrated in Figure 6b. Under incident light of high photon energy, large carrier multiplication in graphene would lead to additional electron/hole pairs being generated (secondary hot-carrier generation); this photoexcitation cascade effect would be more obvious when the incident light contained photons of higher energy. Overall, the vertical-heterojunction graphene/$AuO_x$ photodetector demonstrated broadband, highly efficient, and low-light detection capabilities. In addition, such hot-carrier-assisted photodetectors would provide extra photoresponses under irradiation with high-energy photons.

Finally, we tested the flexibility and mechanical stability of the graphene/$AuO_x$ photodetector. In previous studies, gated three-terminal graphene-based photodetectors did not possess flexibility because they were built on rigid substrates.[10] Figure 7a presents a photographic image of the graphene/$AuO_x$ photodetector recorded during a bending test. By fixing the radius of curvature at 5 mm, we repeated the bending test over 3500 times. Figure 7b displays a plot of the responsivity of the graphene/$AuO_x$ photodetector with respect to the bending time. Here, the wavelength of incident light was 500 nm, the incident power was 0.5 $\mu$W, and the bias was 0.1 V. The responsivity decreased only slightly, from 0.847 to 0.821 A $W^{-1}$ (*ca.* 3.1%), after performing the bending test 3500 times. Therefore, this transparent graphene/$AuO_x$

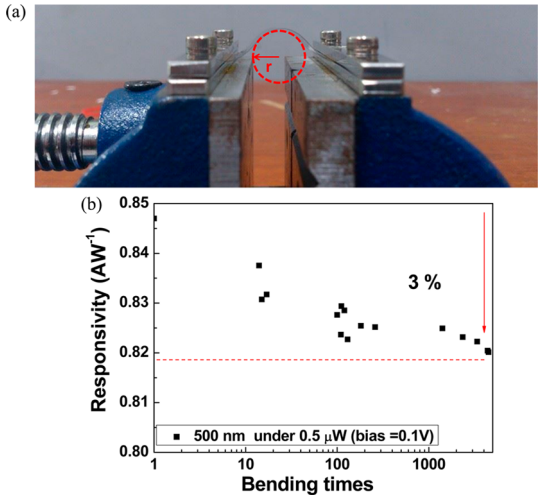


**Figure 7. (a) Photograph of the graphene/$AuO_x$ photodetector during a bending test; radius of curvature (r): 5 mm. (b) Responsivities of the graphene/$AuO_x$ photodetector after bending for various numbers of times ($r$ = 5 mm).**

photodetector possesses good flexibility and stability and has the ability to be integrated with other flexible, wearable electronic devices in the future.

## CONCLUSIONS

In this study, we developed a graphene/$AuO_x$ transparent photodetector, having a detection area on the square-centimeter scale, on a flexible substrate. The $AuO_x$ electrode exhibited high transparency and low reflectance relative to a conventional Au electrode, making it suitable for use in transparent optoelectronic devices. The large-area graphene acted as the active layer for photodetection, as well as a gas-impermeable protecting layer that prevented reduction of the $AuO_x$ electrode. Moreover, the graphene film was "hole-doped" by the underlying $AuO_x$ having a high work function, which can also increase the photoresponse. In addition, graphene/$AuO_x$ photodetector could be operated at a low applied voltage (0.1 V), without the need for back-gating, which is necessary in conventional graphene-based photodetectors. Because of the robust heterojunction formed at the graphene−$AuO_x$ interface, the graphene/$AuO_x$ photodetector exhibited an approximately 10-fold enhancement in responsivity relative to that of the corresponding graphene/Au photodetector. Moreover, the graphene/$AuO_x$ photodetector displayed very efficient, broadband photoresponses from the UV (3300 A $W^{-1}$) to the visible (58 A $W^{-1}$) to the IR (9 A $W^{1-}$) regime. Remarkably, the photodetector exhibited high photoresponse even when the incident power reached as low as the picowatt level in the UV regime and the nanowatt level in the IR regime. In addition, it exhibited linear responses to values of incident power below approximately $2 \times 10^{-10}$, $3 \times 10^{-9}$, and $1 \times 10^{-7}$ W at wavelengths of 310, 500, and 1550 nm, respectively. The large photocurrent in the UV regime was due to both the effective absorption of light and the hot-carrier-assisted photoinduced electric current. The ultrahigh responsivity of this photodetector also facilitated low-light detection. The effective electric field at the graphene−$AuO_x$ interface ensured the efficient separation of electron/hole pairs. Finally, the graphene/$AuO_x$ photodetector featured excellent flexibility and stability. To the best of our knowledge, we are the first to achieve a flexible, large-area, transparent, low-bias, broadband-operable, graphene-based photodetector. Furthermore, our graphene/$AuO_x$ photodetector allowed bifacial operation, detecting light through either front- or rear-side illumination. Therefore, this vertical heterojunction-based graphene/$AuO_x$ photodetector should be compatible with other transparent optoelectronic devices, suggesting applications in the flexible and wearable optoelectronic technologies.

## EXPERIMENTAL SECTION

**Preparation of Graphene and $AuO_x$.** A radio frequency (RF) magnetron reactive sputtering process was used to deposit $AuO_x$, Au, and Ag films on commercial glass and PET substrates. For preparing of $AuO_x$ films, a pure Au target was used. The Ar:$O_2$ gas flow was set at 1:10. The RF power and process pressure were fixed at 100 W and 0.3 Pa, respectively. For deposition of the Au and Ag films, the RF power and chamber pressure were fixed at 50 W and 0.3 Pa, respectively. All the deposition processes were completed at room temperature. A chemical vapor deposition (CVD) system was used to prepare pristine graphene on a copper foil. The CVD-prepared graphene was transferred onto the $AuO_x$ surface using the conventional poly(methyl methacrylate) (PMMA)-transferring process.[27] The PMMA coating was removed with acetone.

**Measurements and Optical Simulation.** Raman spectroscopy and a 532 nm diode laser were used for graphene characterization. Transmittance (T), reflectance (R), and absorbance (A) spectra within the ultraviolet−visible−infrared (UV−vis−IR) regimes were recorded using a Hitachi U4100 spectrophotometer. All electrical measurements were performed using a digital source meter (Keithley 2400). A xenon lamp and a tungsten lamp were the broadband light sources; a monochromator (Horiba Jobin Yvon, iHR-320) was used to obtain monochromated light. The optical constants (refractive index, extinction coefficients) of the $AuO_x$ film were measured using an ellipsometer and the optical thin film model.[28]

*Conflict of Interest:* The authors declare no competing financial interest.

*Supporting Information Available:* The Supporting Information is available free of charge on the ACS Publications website at DOI: 10.1021/acsnano.5b00212.

*Acknowledgment.* We thank the Ministry of Science and Technology, Taiwan, for supporting this study under contracts MOST-103-2221-E-002-041-MY3 and MOST-103-2221-E-002-092-MY3.

## REFERENCES AND NOTES

1. Michel, J.; Liu, J.; Kimerling, L. C. High Performance Ge-on-Si Photodetectors. *Nat. Photonics* **2010**, *4*, 527–534.

2. Xu, C.; Beeler, R. T.; Grzybowski, G.; Chizmeshya, A. V. G.; Menendez, J.; Kouvetakis, J. Molecular Synthesis of High-Performance Near-IR Photodetectors with Independently Tunable Structural and Optical Properties Based on Si-Ge-Sn. *J. Am. Chem. Soc.* **2012**, *134*, 20756–20767.
3. Bao, Q.; Loh, K. P. Graphene Photonics, Plasmonics, and Broadband Optoelectronic Devices. *ACS Nano* **2012**, *6*, 3677–369.
4. Yan, C.; Cho, J. H.; Ahn, J. H. Graphene-Based Flexible and Stretchable Thin Film Transistors. *Nanoscale* **2012**, *4*, 4870–4882.
5. Park, J.; Ahn, Y. H.; Ruiz-Vargas, C. Imaging of Photocurrent Generation and Collection in Single-Layer Graphene. *Nano Lett.* **2009**, *9*, 1742–1746.
6. Lemme, M. C.; Koppens, F. H. L.; Falk, A. L.; Rudner, M. S.; Park, H.; Levitov, L. S.; Marcus, C. M. Gate-Activated Photoresponse in a Graphene P-N Junction. *Nano Lett.* **2011**, *11*, 4134–4137.
7. Xia, F.; Mueller, T.; Lin, Y.-M.; Valdes-Garcia, A.; Avouris, Ph. Ultrafast Graphene Photodetector. *Nat. Nanotechnol.* **2009**, *4*, 839–843.
8. Shi, Y.; Fang, W.; Zhang, K.; Li, L. J. Photoelectrical Response in Single-Layer Graphene Transistors. *Small* **2009**, *5*, 2005–2011.
9. Lv, X.; Huang, Y.; Liu, Z.; Tian, J.; Wang, Y.; Ma, Y.; Liang, J.; Fu, S.; Wan, X.; Chen, Y. Photoconductivity of Bulk-Film-Based Graphene Sheets. *Small* **2009**, *5*, 1682–1687.
10. Mueller, T.; Xia, F.; Avouris, Ph. Graphene Photodetectors for High-Speed Optical Communications. *Nat. Photonics* **2010**, *4*, 297–301.
11. Lee, E. J. H.; Balasubramanian, K.; Weitz, R. T.; Burghard, M.; Kern, K. Contact and Edge Effects in Graphene Devices. *Nat. Nanotechnol.* **2008**, *3*, 486–490.
12. Hsieh, Y. P.; Yen, C. H.; Lin, P. S.; Ma, S. W.; Ting, C. C.; Wu, C. I.; Hofmann, M. Ultra-High Sensitivity Graphene Photosensor. *Appl. Phys. Lett.* **2014**, *104*, 041110.
13. Liu, Y.; Cheng, R.; Liao, L.; Zhou, H.; Bai, J.; Liu, G.; Liu, L.; Huang, Y.; Duan, X. Plasmon Resonance Enhanced Multicolour Photodetection by Graphene. *Nat. Commun.* **2011**, *2*, 579–585.
14. Fang, Z.; Liu, Z.; Wang, Y.; Ajayan, P. M.; Nordlander, P.; Halas, N. J. Graphene-Antenna Sandwich Photodetector. *Nano Lett.* **2012**, *12*, 3808–3813.
15. Furchi, M.; Urich, A.; Pospischil, A.; Lilley, G.; Unterrainer, K.; Detz, H.; Klang, P.; Andrews, A. M.; Schrenk, W.; Strasser, G.; *et al*. Microcavity-Integrated Graphene Photodetector. *Nano Lett.* **2012**, *12*, 2773–2777.
16. Liu, C. H.; Chang, Y. C.; Norris, T. B.; Zhong, Z. Graphene Photodetectors with Ultra-Broadband and High Responsivity at Room Temperature. *Nat. Nanotechnol.* **2014**, *9*, 273–278.
17. Mueller, T.; Xia, F.; Freitag, M.; Tsang, J.; Avouris, Ph. Role of Contacts in Graphene Transistors: A Scanning Photocurrent Study. *Phys. Rev. B* **2009**, *79*, 245430.
18. Zhang, W.; Chuu, C. P.; Huang, J. K.; Chen, C. H.; Tsai, M. L.; Chang, Y. H.; Liang, C. T.; Chen, Y. Z.; Chueh, Y. L.; He, J. H.; *et al*. Ultrahigh-Gain Photodetectors Based on Atomically Thin Graphene-$MoS_2$ Heterostructures. *Sci. Rep.* **2014**, *4*, 3826.
19. Yu, W. J.; Liu, Y.; Zhou, H.; Yin, A.; Li, Z.; Huang, Y.; Duan, X. Highly Efficient Gate-Tunable Photocurrent Generation in Vertical Heterostructures of Layered Materials. *Nat. Nanotechnol.* **2013**, *8*, 952–958.
20. Giovanetti, G.; Khomyakov, P. A.; Brocks, G.; Karpan, V. M.; van den Brink, J.; Kelly, P. J. Doping Graphene with Metal Contacts. *Phys. Rev. Lett.* **2008**, *101*, 026803.
21. Liu, N.; Tian, H.; Schwartz, G.; Tok, J. B.-H.; Ren, T. L.; Bao, Z. Large-Area, Transparent, and Flexible Infrared Photodetector Fabricated Using P-N Junctions Formed by N-Doping Chemical Vapor Deposition Grown Graphene. *Nano Lett.* **2014**, *14*, 3702–3708.
22. Lee, Y. Y.; Tu, K. H.; Yu, C. C.; Li, S. S.; Hwang, J. Y.; Lin, C. C.; Chen, K. H.; Chen, L. C.; Chen, H. L.; Chen, C. W. Top Laminated Graphene Electrode in a Semitransparent Polymer Solar Cell by Simultaneous Thermal Annealing/Releasing Method. *ACS Nano* **2011**, *5*, 6564–6570.
23. Rentenberger, S.; Vollmer, A.; Zojer, E.; Schennach, R.; Koch, N. UV/Ozone Treated Au for Air-Stable, Low Hole Injection Barrier Electrodes in Organic Electronics. *J. Appl. Phys.* **2006**, *100*, 053701.
24. Helander, M. G.; Wang, Z. B.; Greiner, M. T.; Liu, Z. W.; Qiu, J.; Lu, Z. H. Oxidized Gold Thin Films: An Effective Material for High-Performance Flexible Organic Optoelectronics. *Adv. Mater.* **2010**, *22*, 2037–2040.
25. Liu, Y. L.; Fang, C. Y.; Yu, C. C.; Yang, T. C.; Chen, H. L. Controllable Localized Surface Plasmonic Resonance Phenomena in Reduced Gold Oxide Films. *Chem. Mater.* **2014**, *26*, 1799–1806.
26. Berry, V. Impermeability of Graphene and Its Applications. *Carbon* **2013**, *62*, 1–10.
27. Li, X. S.; Zhu, Y. W.; Cai, W. W.; Borysiak, M.; Han, B.; Chen, D.; Piner, R. D.; Colombo, L.; Ruoff, R. S. Transfer of Large-Area Graphene Films for High-Performance Transparent Conductive Electrodes. *Nano Lett.* **2009**, *9*, 4359–4363.
28. Macleod, H. *Thin Film Optical Filters*, 3rd ed.; Institute of Physics Publishing: Bristol, 2001.
29. Entani, S.; Sakai, S.; Matsumoto, Y.; Naramoto, H.; Hao, T.; Maeda, Y. Interface Properties of Metal/Graphene Heterostructures Studied by Micro-Raman Spectroscopy. *J. Phys. Chem. C* **2010**, *114*, 20042–20048.
30. Wang, Y. Y.; Ni, Z. H.; Yu, T.; Shen, Z. X.; Wang, H. M.; Wu, Y. H.; Chen, W.; Wee, A. T. S. Raman Studies of Monolayer Graphene: The Substrate Effect. *J. Phys. Chem. C* **2008**, *112*, 10637–10640.
31. Li, N.; Li, X.; Demiguel, S.; Zheng, X.; Campbell, J. C.; Tulchinsky, D. A.; Williams, K. J.; Isshiki, T. D.; Kinsey, G. S.; Sudharsansan, R. High-Saturation-Current Charge-Compensated InGaAs/InP Uni-Traveling-Carrier Photodiode. *IEEE Photon. Technol. Lett.* **2004**, *16*, 864–866.
32. Britnell, L.; Ribeiro, R.; Eckmann, A.; Jalil, R.; Belle, B.; Mishchenko, A.; Kim, Y.; Gorbachev, R.; Georgiou, T.; Morozov, S. Strong Light-Matter Interactions in Heterostructures of Atomically Thin Films. *Science* **2013**, *340*, 1311–1314.
33. Ju, L.; Velasco, J.; Huang, E.; Kahn, S.; Nosiglia, C.; Tsai, H. Z.; Yang, W.; Taniguchi, T.; Watanabe, K.; Zhang, Y.; *et al*. Photoinduced Doping in Heterostructures of Graphene and Boron Nitride. *Nat. Nanotechnol.* **2014**, *9*, 348–352.
34. Tielrooij, K. J.; Song, J. C. W.; Jensen, S. A.; Centeno, A.; Pesquera, A.; Elorza, A. Z.; Bonn, M.; Levitov, L. S.; Koppens, F. H. L. Photoexcitation Cascade and Multiple Hot-Carrier Generation in Graphene. *Nat. Phys.* **2013**, *9*, 248–252.
35. Shi, H.; Asahi, R.; Stampfl, C. Properties of the Gold Oxides $Au_2O_3$ and $Au_2O$: First-Principles Investigation. *Phys. Rev. B* **2007**, *75*, 205125.
36. Konstantatos, G.; Badioli, M.; Gaudreau, L.; Osmond, J.; Bernechea, M.; de Arquer, F. P. G.; Gatti, F.; Koppens, F. H. L. Hybrid Graphene-Quantum Dot Phototransistors with Ultrahigh Gain. *Nat. Nanotechnol.* **2012**, *7*, 363–368.